



ELSEVIER

Journal of Luminescence 98 (2002) 249–255

JOURNAL OF  
LUMINESCENCE

www.elsevier.com/locate/jlumin

# Monte Carlo simulation of energy transfer rates: application to downward energy transfer within the 825 nm absorption band of the FMO complex of *Prosthechochloris aestuarii*

J.M. Hayes<sup>a,\*</sup>, M. Ruehlaender<sup>b</sup>, C. Soukoulis<sup>b</sup>, G.J. Small<sup>a</sup>

<sup>a</sup>Ames Laboratory, U.S. Department of Energy and Department of Chemistry, Iowa State University, Ames, IA 50014, USA

<sup>b</sup>Ames Laboratory, U.S. Department of Energy and the Department of Physics and Astronomy, Iowa State University, Ames, IA 50011, USA

## Abstract

Splitting of the individual subunit absorptions of the FMO complex of *Prosthechochloris aestuarii* due to disorder is determined by Monte Carlo simulation. The simulations accurately reproduce the 825 nm absorption band and indicate an upper limit for the inter-subunit coupling of  $10\text{ cm}^{-1}$ . From the simulations, rates for downward energy transfer between subunits can be determined using the spectral density determined from hole burning (J. Phys. Chem. B 104 (2000) 9564). On average the splitting between adjacent energy levels is  $\sim 25\text{ cm}^{-1}$  and the energy transfer rate for relaxation between such levels is equal. Relaxation from the top to lowest level is significantly slower. This is in contrast with the experimental finding that relaxation from the top to bottom levels occurs at about twice the rate for the other two relaxations. Further, the rates determined do not agree with the observed variation of zero-phonon hole width and photon echo dephasing times with frequency. The possible involvement of Herzberg–Teller-like dark modes with a peak near  $50\text{ cm}^{-1}$  is discussed. © 2002 Elsevier Science B.V. All rights reserved.

**Keywords:** Energy transfer; Photosynthesis; FMO complex

## 1. Introduction

With the availability of more and better resolved structural data for photosynthetic systems, understanding the details of energy transfer and charge separation in terms of the well-developed concepts of molecular photophysics is now anticipated. Nevertheless, a complete understanding of even some of the best-characterized systems is still elusive. The FMO antenna complex of green sulfur bacteria is a case in point. The atomic

resolution X-ray structure of the FMO complex from *Prosthechochloris aestuarii* has been available since 1974 [1], yet a complete understanding of energy transfer in this system has not yet been attained.

The FMO complex of *P. aestuarii* is a trimeric bacteriochlorophyll *a*-protein complex that mediates energy transfer from the light-harvesting antenna to the reaction center. The complex is a C<sub>3</sub> trimer of identical protein subunits. Each subunit contains a  $\beta$ -sheet with 16 strands that enfold seven BChl *a* pigments with positions and orientations that are repeated in each subunit. Nearest neighbor Mg...Mg distances within a subunit are  $\sim 11$ – $14\text{ \AA}$  and the largest pairwise

\*Corresponding author. Tel.: +1-515-294-4872; fax: +1-515-294-1699.

E-mail address: jmhayes@iastate.edu (J.M. Hayes).

coupling energies are in the 50–200 Å range. The largest coupling between BChl *a* molecules belonging to different subunits is  $\leq 20 \text{ cm}^{-1}$  [2].

More recently, the X-ray structure of another species of green sulfur bacteria, *Chlorobium tepidum*, has also been determined [3]. The relative orientations of the BChl *a* molecules and the distances between them are very similar to those of *P. aestuarii*. However, the 4.2 K absorption spectra of the FMO complexes of the two species show significant differences. These are most likely due to differences in the excitation energies of one or more of the BChl *a* molecules of the subunit, which may be related to differences in H-bonding and BChl *a*/residue differences in the two species.

Because of the detailed structural information, the FMO complex has been attractive for the study of excitonic effects. However, because the seven BChl *a* molecules in a subunit are energetically inequivalent and there is no reliable method for calculating the site energies, the problem is not as simple as it is for more symmetric photosynthetic systems. For example, in contrast with the FMO complex, in the circular B850 aggregate of LH2 antenna containing 16 or 18 BChl *a*, there are only two inequivalent BChl *a* pigment sites. For the FMO complex, the exciton calculations of Lu and Pearlstein [4], Gülen [5], and Louwe et al. [6] indicated that the  $Q_y$  states are mini-excitons with the excitation shared by two or three molecules at most. There is general agreement that the 825 nm band is due to three states that stem from the lowest energy  $Q_y$ -state of each subunit. For this state, excitation resides to a large extent on a single molecule. However, there is disagreement as to which of the seven BChl *a* molecules has the lowest site energy. Lu and Pearlstein [4] assign BChl *a* 7 as the lowest while Gülen [5] and Louwe et al. [6] assign it as BChl *a* 6 and BChl *a* 3, respectively. At present, the model of Louwe et al. [6] appears to give the best fit to the absorption, circular dichroism, linear dichroism, and triplet minus singlet difference spectra at low temperatures. In their work [6], they argue that the inter-subunit coupling is too weak ( $\leq 10 \text{ cm}^{-1}$ ) to warrant consideration of trimer states.

The 825 nm absorption band, of interest here, appears mainly to be localized on a single BChl *a*.

In the model of Louwe et al. [6] this is BChl *a* 3. Thus, underlying this band there are three transitions, one for each monomer. Evidence for these three bands arises from hole burning of both *C. tepidum* and *P. aestuarii* [7–9] and from photon echo [10] studies which find that the lifetime determined values measured for red edge excitation increase as the excitation energy increases across the absorption band. In the hole burning work [7,8], this increase was attributed to inter-subunit energy transfer. In analyzing this relaxation, a curious result is obtained. Two assumptions are made: that excitation in the middle of the band excites predominantly the middle of the three subunit transitions while blue excitation excites predominantly the highest energy of the three inter-subunit bands, and that the levels are nearly equally spaced energetically. With these assumptions, it is concluded that relaxation directly from the highest level to the lowest level is twice as fast as the other two relaxation processes, i.e., from the highest to the middle level, or from the middle to the lowest level. This is unexpected as the energy gap for relaxation from the highest level to the bottom level is twice that of the other two splittings.

In this paper, the relaxation dynamics are investigated by Monte Carlo simulation of the three subunit bands that contribute to the 825 nm absorption band. From these simulations, the relaxation rates can be calculated. These calculations are aided by detailed knowledge of the spectral density needed to determine the relaxation rates. The spectral densities are known from hole burning throughout the 825 nm band [7]. Two possible energy transfer mechanisms are considered. The first is Förster energy transfer in which the modes active in the spectral density are considered to be localized, i.e., not spatially extended. On the other hand, the case of delocalized phonon modes that encompass both the energy donor and the energy acceptor is also considered. Förster energy transfer has been applied to many photosynthetic systems [11–13], while the involvement of delocalized modes is less often studied. Although the distances between BChl *a* molecules in different subunits in the FMO complex are such ( $> 25 \text{ Å}$ ) that delocalized

modes are unlikely, they are considered for completeness.

## 2. Theory and calculation methods

The lowest energy band of the FMO absorption is due to three BChl *a* molecules, one in each of the subunits that make up the trimer. These were assigned as BChl *a* 7 by Pearlstein [4], as BChl *a* 6 by Gülen [5], and as BChl *a* 3 by Louwe et al. [6]. It is reasonable to expect that the coupling between symmetry related BChl *a* in different subunits is weak ( $\leq 10 \text{ cm}^{-1}$ ), thereby justifying the exciton calculations on only a single subunit as done by Louwe et al. These calculations implicitly assume that the energies of the equivalent BChl *a* of each subunit are the same. However, the effects of disorder will cause these energies to vary within subunits. To gauge the effects of disorder, a Monte Carlo simulation is used. The eigenvalues of the interaction matrix

$$\begin{bmatrix} E + d_1 & V_{DA} & V_{DA} \\ V_{DA} & E + d_2 & V_{DA} \\ V_{DA} & V_{DA} & E + d_3 \end{bmatrix} \quad (1)$$

are found. Here,  $E$  is the energy of the lowest energy absorption of BChl *a* in a subunit;  $V_{DA}$  is the coupling between these BChl *a* in different subunits; and  $d_i$ ,  $i = 1, 2, 3$  are the shifts in energy due to disorder. The  $d_i$  are selected randomly from Gaussian distributions whose widths,  $\Gamma$ , are varied so that the sum of the distributions of energy that result from the solutions of Eq. (1), replicate the experimentally observed lowest energy absorption band of the complex.

From determination of the eigenvalues of Eq. (1) with various couplings,  $V_{DA}$ , and widths,  $\Gamma$ , of the underlying distributions followed by comparison with the experimental absorption,  $V_{DA}$  and  $\Gamma$  can be determined. The Monte Carlo simulations then give the energies of the individual absorptions for the three BChl *a* for the number of molecules in the calculation. Here, 5000 molecules were simulated. The energy splittings between the three BChl *a* making up each of the 5000 trimers can then be determined. From knowledge of these,

one would like to calculate the rate of energy transfer from the higher energy BChl *a* to the lower energy BChl *a* in the same trimer.

The initially excited molecule is identified as the donor, with ground state,  $D$ , and excited state,  $D'$ . The BChl *a* molecule to which the excitation is transferred is the acceptor with ground and excited states,  $A$  and  $A'$ , respectively. In the case of localized modes, the phonon or vibrational coordinates are those of the two molecules. Thus for the donor the ground state mode is signified as  $d$ , and in the excited state as  $d'$ . Similarly for the acceptor, the ground and excited state modes are  $a$  and  $a'$ . The initial state is then  $D'Aa$  and the final state  $DdA'a'$ . A generalized expression for the energy transfer rate between these two states can be given in the Condon approximation as

$$k(\Omega; T) = 2\pi V_{DA}^2 \sum_{d',d} | \langle d|d' \rangle |^2 | \langle a'|a \rangle |^2 \times \delta(\Omega + (\omega_{d'} + \omega_a) - (\omega_d + \omega_{a'})). \quad (2)$$

Here,  $\Omega = (E_{D'} - E_A)/\hbar$ ,  $Av_i (i = d', a)$  denotes the thermal average over these modes, and  $V_{DA}^2$  is the dipole–dipole interaction between the two BChl *a*. Defining

$$G(\Omega) = \sum_{d',d} | \langle d|d' \rangle |^2 | \langle a'|a \rangle |^2 \times \delta(\Omega + (\omega_{d'} + \omega_a) - (\omega_d + \omega_{a'})),$$

one can write

$$k(\Omega; T) = 2\pi V_{DA}^2 \langle G(\Omega) \rangle_T \quad (3)$$

in energy units of circular frequency. Writing the Dirac delta function in Eq. (2) as

$$\int d\Lambda \delta(\Lambda - [\omega_{D'} + \omega_{d'}] + \omega_d) \times \delta(\Lambda - [\omega_{A'} + \omega_{a'}] + \omega_a) \quad (4)$$

yields

$$k(\Omega; T) = 2\pi V_{DA}^2 \int d\Lambda \left\{ Av_{d'} \sum_d | \langle d|d' \rangle |^2 \times \delta(\Lambda - [\omega_{D'} + \omega_{d'}] + \omega_d) \right\} \times \left\{ Av_a | \langle a'|a \rangle |^2 \delta(\Lambda - [\omega_{A'} + \omega_{a'}] + \omega_a) \right\}. \quad (5)$$

The two terms in Eq. (5) within the  $\{ \}$  are proportional to the normalized fluorescence and

the normalized absorption. (See reference [13] for details.) Thus for localized phonons, the usual Förster result is obtained, i.e., the rate is proportional to the overlap integral of the normalized fluorescence and absorption spectra.

For delocalized phonons, the initial and final states may be designated as  $D'A\eta'$  and  $DA'\eta$ , respectively. Here  $\eta$  represents the delocalized modes. Now the rate is given by

$$k(\Omega; T) = 2\pi V_{DA}^2 A v \sum_{\eta'} |\langle \eta | \eta' \rangle|^2 \times \delta(\Omega - [\omega_{\eta} - \omega_{\eta'}]). \quad (6)$$

In the low-temperature limit ( $T \rightarrow 0$  K),  $\eta' = 0$  and

$$k(\Omega; 0 \text{ K}) = 2\pi V_{DA}^2 \sum_{\eta} |\langle \eta | 0 \rangle|^2 \delta(\Omega - \omega_{\eta}) \quad (7)$$

with  $\Omega$  as previously defined. Now

$$G(\Omega) = \sum_{\eta} |\langle \eta | 0 \rangle|^2 \delta(\Omega - \omega_{\eta}),$$

and the delta function is equal to  $\int dA \delta(A - \omega_{D'} + \omega_{\eta}) \delta(A - \omega_{A'})$ . Substituting this into Eq. (7) results in

$$k(\Omega; 0 \text{ K}) = 2\pi V_{DA}^2 \int dA \left[ \sum_{\eta} |\langle \eta | 0 \rangle|^2 \times \delta(A - \omega_{D'} + \omega_{\eta}) \right] \delta(A - \omega_{A'}). \quad (8)$$

Now the term in square brackets is again proportional to the normalized fluorescence spectrum. The meaning of the final Dirac delta function then is to evaluate the fluorescence at  $A = \omega_{A'}$ . Thus, the two energy transfer mechanisms considered differ but each requires knowledge of the spectral density, i.e., the single site absorption and fluorescence spectrum of the BChl *a* in the FMO complex.

Knowing the splittings and widths of the distribution of energies of the lowest energy BChl *a* in each monomer from the disorder calculation, a macroscopic sample is simulated by randomly selecting one energy from each distribution and assigning that triad of energies to an individual trimeric complex. This is repeated for a large number (5000) of complexes. In this way, a  $5000 \times 3$  matrix is produced. The rows of the

matrix represent one trimeric complex of the ensemble, the columns are the energies of the three lowest energy BChl *a*, (one in each monomer) of that trimer.

Within a complex, the energies are uncorrelated. Thus, there is a distribution of energy gaps between the components of the complex. From the energy gaps, the energy transfer rate can be calculated, if the spectral density is known. In Ref. [7], analysis of the hole structure as a function of burn wavelength throughout the 825 nm band was used to determine the spectral density. It was shown that there are several low-frequency modes that contribute to the spectral density. Below  $100 \text{ cm}^{-1}$ , the mode frequencies reported in Ref. [7] were 18, 24, 36, 48, and  $72 \text{ cm}^{-1}$ . Huang–Rhys factors for these modes were reported as 0.24, 0.05, 0.12, 0.04, and 0.12, respectively. Similar mode structure has also been reported in the line narrowed fluorescence spectrum although, in that work, the 24 and  $48 \text{ cm}^{-1}$  modes were not resolved. Although in Ref. [7], the hole spectra simulations included all five low-frequency modes, here a somewhat simpler spectral density is used to decrease the time required for calculation of the overlap integrals. In this approximation, the four lowest frequency modes are replaced by a single mode at  $25 \text{ cm}^{-1}$  with a Huang–Rhys factor of 0.36 and a width of  $20 \text{ cm}^{-1}$ . For both this band and the  $72 \text{ cm}^{-1}$  band (with Huang–Rhys factor of 0.12 and width of  $12 \text{ cm}^{-1}$ ), Gaussian shapes are used. These approximations yield a spectral density that is less structured than that experimentally observed, but it does fairly well reproduce the envelope of the measured spectral density.

In the overlap calculations, it is assumed that the fluorescence and absorption bands of the individual molecules are mirror symmetric. That this is approximately so can be inferred from the hole and fluorescence line narrowed spectra. The overlap integrals for the 5000 complexes in the simulation are calculated with the MathCad program.

### 3. Results

In Fig. 1, is shown the experimental absorption spectrum along with the simulated number density

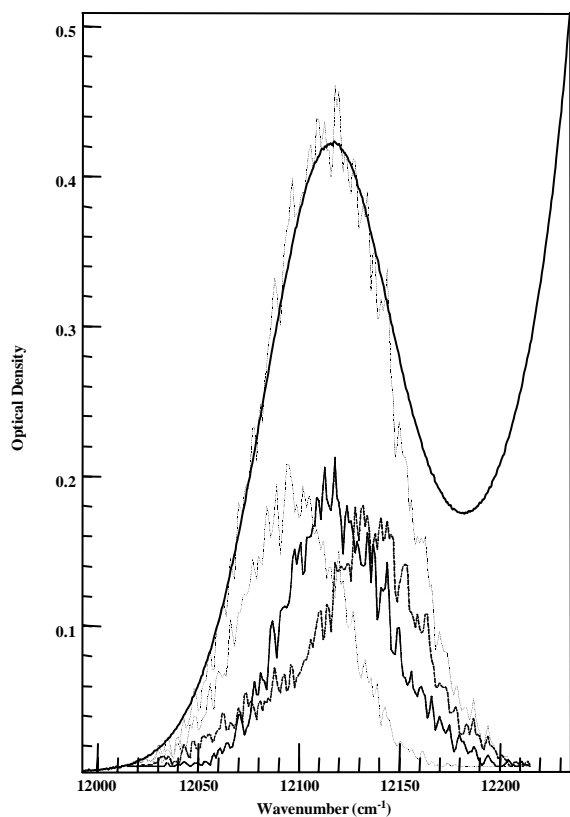


Fig. 1. The solid curve is the low-energy region of the experimental absorption spectrum of the FMO complex of *P. aestuarii* at 4.2 K. Beneath this are the three number density curves obtained from solution of the interaction matrix. These are scaled so that the peak of their sum, shown superimposed on the absorption spectrum, matches the peak optical density of the absorption.

of the three distributions obtained by diagonalization of the energy matrix and the sum of the number densities. The number densities are proportional to the absorption spectrum. The data are shown on a wavenumber scale relative to the peak of the absorption spectrum ( $12117\text{ cm}^{-1}$  for *P. aestuarii*). A good fit is obtained for the experimental absorption using a standard deviation,  $\sigma$ , of  $30\text{ cm}^{-1}$ . This corresponds to a full width at half maximum of  $70.6\text{ cm}^{-1}$ . The curves shown were obtained with a coupling energy,  $V_{DA}$ , of  $6\text{ cm}^{-1}$ . However, identical fits are obtained for the same distribution with any value of coupling energy for which  $V < \sim \sigma/3$ . Thus, only an upper

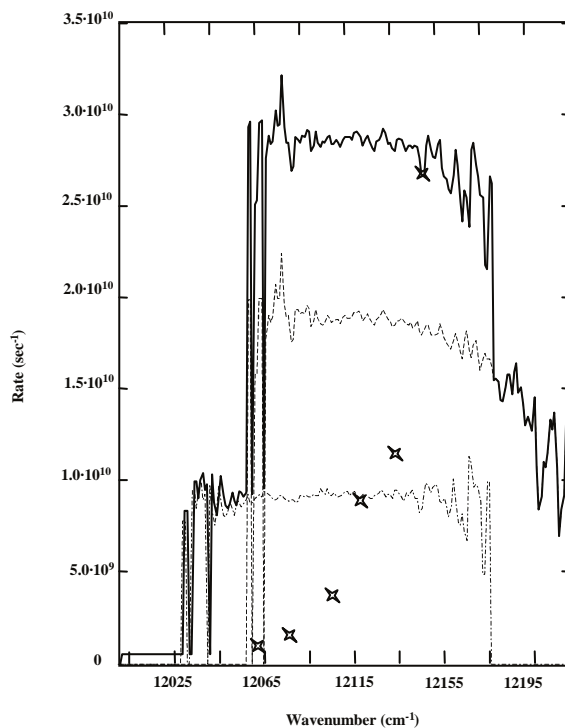


Fig. 2. The top curve is the total relaxation rate due to energy transfer, calculated as described in the text. The middle curve is the calculated relaxation from the highest energy BChl *a* and the bottom curve is the relaxation rate from the BChl *a* with the middle energy. The rates are scaled so that the total rate at  $12151\text{ cm}^{-1}$  is equal to the rate determined from the hole width at this frequency. The hole width determined values are shown as X's.

bound for  $V$  can be determined. Based on Fig. 1 and similar results,  $V_{DA}$  must be  $< 10\text{ cm}^{-1}$  and  $\sigma \approx 30\text{ cm}^{-1}$ .

For these values of  $V_{DA}$  and  $\sigma$ , one of the distributions describing the absorption energy of the three lowest energy absorbing BChl *a* is at the peak of the unresolved absorption and the other two are shifted  $-17$  and  $+26\text{ cm}^{-1}$  from the absorption maximum. The three bands are close to Gaussian and of nearly equal intensity although the highest energy band is slightly weaker. As shown in Fig. 1, the sum of the three bands gives a good fit to the 825 nm band of the FMO complex.

Fig. 2 shows the results of calculating the overlap integrals for the various energy splittings that occur in the 5000 complexes. The three "rate"

curves in the figure are determined as follows. For each energy interval of  $1\text{ cm}^{-1}$  (chosen to correspond to the experimental resolution) the overlaps for molecules with absorption in that interval are summed. The total rate calculated in this way is the top curve of Fig. 2. The other rate curves shown are for overlaps only for the lowest and middle energy molecules of each complex, ( $k_{2\rightarrow 1}$ , lowest curve), and for the two overlaps of the highest absorbing molecule of each complex, ( $k_{3\rightarrow 1}, k_{3\rightarrow 2}$ , middle curve). All of the rates are scaled so that the total rate at  $12151\text{ cm}^{-1}$  is equal to the rate determined from the experimental zero-phonon hole width measured at that energy. Rates determined from hole widths at several wavelengths are shown in the figure.

The simulated rates shown were calculated from the overlap integrals. Thus, they represent the Förster (localized) rate. Note that by calculating the relative rates and then scaling to an experimental value, knowledge of factors such as the refractive index is not necessary. As pointed out by Knox [14], the correct value to use for the refractive index is a complicated matter.

Several things are evident from the simulated rate curves. First, only at the very red, low-absorption edge of the band is it possible to cleanly excite only the lowest absorbing BChl *a* that is incapable of energy transfer. None of the holes shown are in this region. Second, note that due to the averaging of the rates over the number of molecules in each energy interval, the edges of the rate curve exhibit step behavior as the mid-energy and high-energy distributions “turn on”. Third, except for these edge regions, the rates are flat across the absorption band with  $k_3 \equiv k_{3\rightarrow 1} + k_{3\rightarrow 2} \approx 2k_{2\rightarrow 1}$ . The average rates  $\langle k_{3\rightarrow 2} \rangle$  and  $\langle k_{2\rightarrow 1} \rangle$  are nearly equal while  $\langle k_{3\rightarrow 1} \rangle$  is only slightly smaller.

In contrast, the experimental hole widths show a marked increase with absorption energy. Further, if, as done in Refs. [7,8], it is assumed that  $k_{2\rightarrow 1} \approx k_{3\rightarrow 2}$  then from the hole widths,  $k_{3\rightarrow 1}$  is found to be  $\sim 2k_{3\rightarrow 2}$ . The calculations do justify this assumption, as the average energy gaps for adjacent levels are nearly equal at  $27\text{--}28\text{ cm}^{-1}$ . Calculations with other forms of the spectral density show that in order for  $k_{3\rightarrow 1}$  to be

$> k_{3\rightarrow 2}$ , it is necessary for the spectral density to be greater in the region of  $\Delta E_{31}$  than in the region of  $\Delta E_{32}$ . Such a spectral density is not consistent with either line narrowed fluorescence or hole spectra. Simulations based on the delocalized mode theory were also performed. These also showed a relatively flat rate when scaled in a manner very similar to the Förster rates. Thus, it is not possible to distinguish between the localized and delocalized mode models.

That the calculated rates do not account for the strong dependence of the hole width (or photon echo dephasing times [10]) on the burn frequency is perplexing. Again, one can be confident in the experimental spectral density associated with the Franck–Condon factors of low-energy modes. Although only an approximate spectral density is used, the results are not sensitive to the frequencies or Huang–Rhys factors in the region from 18 to  $48\text{ cm}^{-1}$ . At this time, we can think of only one plausible explanation for the discrepancy. It is that there are “dark” low-frequency modes (inactive in absorption) that promote downward energy transfer. In this case one has to go beyond the Condon approximation to consider the modulation of the electronic coupling by nuclear motions (see, e.g. [15,16]). The situation is analogous to Herzberg–Teller vibronic coupling in molecules. The dark modes could act in concert with the Condon modes to provide a new spectral density. For it to explain the hole width data, it would have to exhibit a prominent peak at  $\sim 50\text{ cm}^{-1}$  and relatively weak spectral density near  $\sim 25\text{ cm}^{-1}$ . With  $k_{3\rightarrow 1}$  being considerably  $> k_{3\rightarrow 2}$  (and  $k_{2\rightarrow 1}$ ), the hole width data could be explained. The problem, of course, is that since the promoting modes are dark, the model cannot be tested. Even if their frequencies were known, one would be faced with calculating the HT-like energies, a formidable theoretic problem. Finally, single FMO complex studies with sufficient statistics should prove useful since the spectral density could be directly determined.

### Acknowledgements

Research at the Ames Laboratory was supported by the Division of Chemical Sciences,

Office of Basic Energy Sciences, US Department of Energy. Ames Laboratory is operated for USDOE by Iowa State University under Contract W-7405-Eng-82.

## References

- [1] R.E. Fenna, B.W. Matthews, J.M. Olson, E.K. Shaw, *J. Mol. Biol.* 84 (1974) 231.
- [2] R.M. Pearlstein, *Photosynth. Res.* 31 (1992) 213.
- [3] Y.F. Li, W. Zhou, R.E. Blankenship, J.P. Allen, *J. Mol. Biol.* 271 (1997) 456.
- [4] X. Lu, R.M. Pearlstein, *Photochem. Photobiol.* 57 (1993) 86.
- [5] D. Gülen, *J. Phys. Chem.* 100 (1996) 17684.
- [6] R.J.W. Louwe, T. Vrieze, A.J. Hoff, T.J. Aartsma, *J. Phys. Chem. B* 101 (1997) 11273.
- [7] S. Matsuzaki, V. Zazubovich, M. Rätsep, J.M. Hayes, G.J. Small, *J. Phys. Chem. B* 104 (2000) 9564.
- [8] M. Rätsep, R.E. Blankenship, G.J. Small, *J. Phys. Chem. B* 103 (1999) 5736.
- [9] E.M. Franken, S. Narken, R.J.W. Louwe, T. Amesz, T.J. Aartsma, *Biochemistry* 37 (1998) 5046.
- [10] R.J.W. Louwe, T.J. Aartsma, *J. Phys. Chem. B* 101 (1997) 7221.
- [11] W.S. Struve, in: R.E. Blankenship, M.T. Madigan, C.E. Bauer (Eds.), *Anoxygenic Photosynthetic Bacteria*, Kluwer, Dordrecht, 1995, pp. 297–313.
- [12] H. van Amerongen, R. van Grondelle, *J. Phys. Chem. B* 105 (2001) 604.
- [13] V. May, O. Kühn, *Charge and Energy Transfer Dynamics in Molecular Systems*, Wiley-VCH, Berlin, 2000, pp. 382–386.
- [14] R.S. Knox, private communication.
- [15] A.S. Davydov, *Theory of Molecular Excitons*, Plenum Press, New York, 1971.
- [16] H. Port, D. Rund, G.J. Small, V. Yakhot, *Chem. Phys.* 39 (1979) 175.